Front. Chem. Sci. Eng. 2017, 11(3): 328–337
DOI 10.1007/s11705-017-1646-y

RESEARCH ARTICLE

The preparation and performance of lignin-based activated carbon fiber adsorbents for treating gaseous streams

Min Song (✉)[1], Wei Zhang[2], Yongsheng Chen[3], Jinming Luo[3], John C. Crittenden[3]

1 Key Laboratory of Energy Thermal Conversion and Control (Ministry of Education), School of Energy and Environment, Southeast University, Nanjing 210096, China
2 State Environmental Protection Key Laboratory of Environmental Risk Assessment and Control on Chemical Process, School of Resources and Environmental Engineering, East China University of Science and Technology, Shanghai 200237, China
3 Brook Byers Institute for Sustainable System, School of Civil and Environmental Engineering, Georgia Institute of Technology, Atlanta, GA 30332-0595, USA

Abstract Two types of lignin-based carbon fibers were prepared by electrospinning method. The first was activated with Fe_3O_4 (LCF-Fe), and the second was not activated with Fe_3O_4 (LCF). Gas phase adsorption isotherms for toluene on LCF-Fe and LCF were studied. The gas phase adsorption isotherm for 0% RH showed LCF-Fe have about 439 mg/g adsorption capacity which was close to that of commercially available activated carbon (500 mg/g). The Dubinin-Radushkevich equation described the isotherm data very well. Competitive adsorption isotherms between water vapor and toluene were measured for their RH from 0 to 80%. The effect of humidity on toluene gas-phase adsorption was predicted by using the Okazaki et al. model. In addition, a constant pattern homogeneous surface diffusion model (CPHSDM) was used to predict the toluene breakthrough curve of continuous flow-packed columns containing LCF-Fe, and its capacity was 412 mg/g. Our study, which included material characterization, adsorption isotherms, kinetics, the impact of humidity and fixed bed performance modeling, demonstrated the suitability of lignin-based carbon fiber for volatile organic compound removal from gas streams.

Keywords lignin, carbon fiber, electrospinning, toluene, humidity

1 Introduction

Different methods have been used in removing volatile organic compounds (VOCs) from gaseous streams, such as adsorption, condensation, catalytic oxidation and thermal oxidation [1]. The adsorption of VOCs onto adsorbents is an effective treatment process for low concentration levels (ppm) [2,3]. The performance of adsorption depends on the equilibrium capacity, kinetics and the impact of relative humidity (RH). A good adsorbent must have a large surface area and abundant pore structure. The presence of water vapor exhibits the obvious effect on the adsorption of VOCs; at low RH, less adsorption of water occurs; at high RH, water hinders the adsorption of VOCs. So it is necessary to select the fine adsorbent with a low capacity of water at high relative humidity.

Activated carbons are well known as excellent adsorbents for the removal of VOCs due to their large surface areas with large pore volumes [4,5]. Among activated carbons, activated carbon fiber (ACF) exhibits the unique advantage to remove the VOCs. It exhibits the higher adsorption capacity than other adsorbents, which is ascribed to its high BET surface area and large pore size distribution [6,7]. Bio-renewable and bio-derived sources such as agricultural residues and forest products have been used as precursors of activated carbon-fiber extensively [8]. The low cost and high availability of lignin makes it as an excellent precursor for the production of activated carbon [9,10]. Among the various preparation methods, electrospinning is a simple and versatile method. It is suitable for the production of high performance fibrous materials with small diameters, abundant porosity, and high surface area. Electrospinning also offers excellent flexibility in producing fibers for a wide range of applications [11]. Therefore, electrospinning method was used to synthesize lignin based carbon fibers.

The incorporation of the metal particles on the surface of carbon materials could alter their surface chemistry

Received September 8, 2016; accepted March 21, 2017

E-mail: minsong@seu.edu.cn

properties, but preserving the properties of the carbon matrix. The excellent sorption ability of these materials is linked to the catalytic action of metals. Fe_3O_4 catalyst is a well-known catalyst, which produces high-performance activated carbons during activation. In addition, the incorporate Fe_3O_4 into porous supporting materials such as activated carbon, graphene could prevent their agglomeration into larger ones [12].

The adsorption performance is not only related to the adsorbent but also the characteristics of adsorbate (i.e., saturation vapor pressure and polarizability). Accordingly, lower vapor pressure and larger polarizability is favorable to adsorption. Many studies have identified excellent isotherms for the adsorption of VOCs on ACF [13,14]. In addition, it has been reported that water vapor could reduce the adsorption capacity for VOCs [15,19]. Consequently, it is important to prepare an activated carbon that can perform well at high RH. The best activated carbons will have very few hydrophilic sites (e.g., oxygen containing functional groups on the surface) and will not adsorb water vapor at low RH. However, at high RH, the adsorption of VOCs is hindered due to the filling of water into the carbon pores by capillary condensation. Accordingly, it is important to prepare ACFs that have as few hydrophilic sites as possible.

Therefore, we prepared ACFs from lignin using electrospinning and evaluated their performance. The major objectives of this study were to: (1) prepare highly efficient lignin based carbon fiber adsorbents using electrospinning, (2) develop an experimental protocol to measure gas phase equilibrium isotherm data, (3) determine the gas phase isotherms capacity for toluene under dry and humid conditions, (4) evaluate the effect of humidity on gaseous adsorption capacities, (5) validate models for gaseous adsorption equilibria of VOCs and the impact of RH, and (6) predict the breakthrough curves using a constant pattern homogeneous surface diffusion model (CPHSDM).

2 Materials and methods

2.1 Raw materials

Lignin alkali and polyvinyl alcohol (PVA) were all purchased from Sigma-Aldrich (St. Louis, MO, USA), which were used to prepare solutions for electrospinning. The proximate and ultimate analysis of lignin is shown in Table 1. The acetic acid (ACS reagent$\geqslant$99.7%) was purchased from Sigma-Aldrich. All other reagents were also purchased in analytical grade from Sigma-Aldrich. All solutions were freshly prepared with ultrapure water.

2.2 Electrospinning

Lignin alkali was used as the carbon fiber precursor. In this process, original acetic acid was used as the lignin solvent and 1 g lignin was dissolved in 3 mL acetic acid to obtain the lignin solution. And then, the solutions were agitated at 60 °C for 15 min, cooled to room temperature and stirred for 120 min. 15 wt-% PVA aqueous solutions were prepared. Then, 1 mL PVA solution was added to 3 mL lignin solution to form a mixture solution. The mixture was ultrasonicated for 1 h, and then used as the spinning solution to synthesize the lignin-based fiber (LF) after cooling to room temperature. In addition, 50 mg Fe_3O_4 catalyst were added into the mixture solution to synthesize the lignin based fiber with Fe_3O_4 (LF-Fe).

The above suspensions used for electrospinning are loaded into a 10 mL syringe with a 22-gauge needle. The electrospinning process was operated under voltage of 18 kV and a flow rate of 0.4 mL/min. An aluminum cylinder covered with aluminum foil was used as a collector. The prepared electrospinning fibers were collected and dry overnight at room temperature in a desiccator.

2.3 Peroxidation and activation

The lignin-based fibers with and without Fe_3O_4 (LF and LF-Fe) were first peroxided in a tubular furnace under air atmosphere. The lignin-based fibers were heated from room temperature to 200 °C with the rate of 0.5 °C/min, kept at 200 °C for 36 h during the peroxidation process. Subsequently, the thermos-stabilized fibers were activated under a nitrogen atmosphere at 600 °C for 90 min. The heating rate during activation was 10 °C/min. Samples were then cooled to room temperature to form carbon fibers with and without Fe_3O_4. The activated carbon fibers that were activated with the Fe_3O_4 catalyst were washed with ultrapure water to remove the Fe, and then dried.

2.4 Characterization

Brunauer-Emmett-Teller (BET) surface areas and pore structure parameters were acquired by Micromeritics ASAP 2020 with nitrogen adsorption at 77 K. Fourier transform infrared spectroscopy (FTIR) (Bruker Tensor 27) was used to analyze the composition of prepared carbon fiber in the range of (500 to 4000) cm^{-1}. The point

Table 1 The proximate and ultimate analysis of lignin[a)]

Sample	A_{ad}/%	M_{ad}/%	C_{ad}/%	H_{ad}/%	N_{ad}/%	S_{ad}/%	O_{ad}/%
Alkali lignin	18.29	10.56	46.80	4.107	0.02	3.887	16.34

a) ad: air dry

of zero charge for activated carbon surfaces was assessed by titration. Carbon, hydrogen, sulfur and nitrogen contents of prepared carbon fibers were measured by Elemental Analyzer (Perkin-Elmer, Norwich, CT, USA). The proximate analysis is determined according to the GB/T212-2008 method. The amount of oxygen is determined by the balance according to Equation:

$$C_{ad} + H_{ad} + O_{ad} + N_{ad} + S_{ad} + A_{ad} + M_{ad} = 100$$

2.5 Adsorption isotherm procedure

Gas phase isotherm procedure. We used the constant volume method to measure gas phase equilibrium data, which involved using a bottle as a constant volume batch reactor to which known amounts of toluene, water vapor and activated carbon were added (Adsorption isotherms were measured by Ryu et al. [20] using this method [21,22]). 0.5 g adsorbents were weighed and placed at the bottom of a glass bottle. The bottles were purged with high-purity nitrogen. The pressure was kept at one atmosphere. The pressure inside the bottle was measured using a U-manometer. One port was connected to the exhaust port of the bottle. The other port was opened to achieve a final pressure of one atmosphere.

Different volumes of gaseous toluene were injected into the glass bottle by using a syringe with a side-port needle to acquire the desired initial concentration. The injected quantities of toluene depended on the desired initial gas-phase concentration. 18 μL toluene solutions were injected into 155 mL glass bottle to acquire the initial concentration of gaseous toluene. All of the glass bottles were equilibrated under room temperature. After 1 h, the gas toluene in each glass bottle was analyzed by using gas chromatography.

Liquid-phase isotherm procedure. 0.1 g carbon samples were mixed with 100 mL of toluene aqueous solution in a 250 mL flask, and the flask was shaken for 12 h in a temperature-controlled water bath at 20 °C. The initial concentration for toluene was 10, 30, 50, 70, and 100 mg/L, respectively. The amount adsorbed was determined from the initial and final concentration in the liquid.

2.6 Analytical procedure

Toluene concentration was measured using a gas chromatograph (HP 5890) with a flame ionization detector (FID). The column of the gas chromatograph was 30 m in length, 0.1 mm I.D., and 0.1 μm film thicknesses narrow bore column (DB-5). The GC oven was hold at 40 °C for 2 min, and then heated from 40 to 120 °C at the rate of 10 °C/min, subsequently hold at 120 °C for 2 min. The carrier gas (N_2) flow rate was 2.3 mL/min. The N_2 make-up gas, H_2 gas and oxidizing gas (air) were used by the FID detector at a flow rate of 20 mL/min, 30 mL/min, 300 mL/min respectively. The detector temperature was 250 °C. The retention time of toluene was 3.4 min.

3 Results and discussion

3.1 Characteristics of the lignin-based carbon fiber adsorbents

The pure lignin solution is difficult to produce fibers by electrospinning. The PVA was used as an adhesive for lignin. The mixing of PVA solution with lignin could enhance viscosity of solution. However, high concentration PVA solution could cause the lignin aggregation in mixture solution. The 15 wt-% polyvinyl alcohol (PVA) aqueous solution was selected as the dispersant for its outstanding biocompatibility and water solubility.

Lignin has a glass transition temperature which is far below the temperatures required for carbonization; therefore the lignin fibers must be pretreated before further processing to prevent softening and fusion [11]. The thermos stabilization of lignin fibers under air could make the water and acetic acid contained in original fibers volatilize. And then surface carbon of fiber is oxidized to higher valence oxygen-containing group, which could prevent the raw fibers melting and keep the fibroid shape during the subsequent carbonization step [23]. While for carbonization, it's to consolidate the carbonaceous structure of fibers; in addition, carbonization of the stabilized lignin nanofibers produces an increase in the carbon content. The carbonization temperature takes our previous research as reference [24].

Figure 1 shows the SEM photographs of lignin based carbon fiber in the absence and presence of Fe_3O_4. The results show that the diameter of the lignin carbon fibers is about 1 μm. After the activation with Fe_3O_4, there are scattering of metal compounds particles on the surface of carbon fiber. Furthermore, the diameter of carbon fiber decrease to about 700–900 nm in the presence of Fe_3O_4.

The structures of oxygen containing groups were analyzed by a Fourier transform infrared spectrometer. The absorption peaks illustrate the presence of some surface functional groups. Figure 2 compares FTIR spectra of the carbon fiber adsorbents before and after activation. The main intensity peaks presented in Fig. 2 were summarized in Table S1 [12,24]. The FTIR curves of LF and LF-Fe look similar, indicating the similar structures and functional groups on their surface. However, LCF and LCF-Fe exhibit the different intensities and a slight shift in wavenumbers, suggesting their small differences in the surface chemistry. The peak located at 876 cm^{-1} represents the guaiacyl functional groups of lignin. The 1100 cm^{-1} is ascribed to the C–H vibration of the syringyl group in lignin. The strong absorption band observed at 1020 cm^{-1}

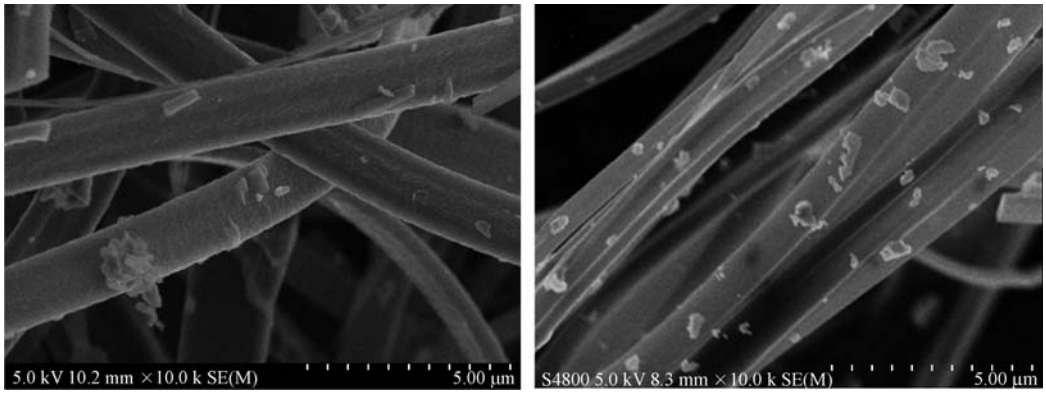

Fig. 1 The SEM images of lignin carbon fiber in the absence (left) and presence of Fe_3O_4 (right)

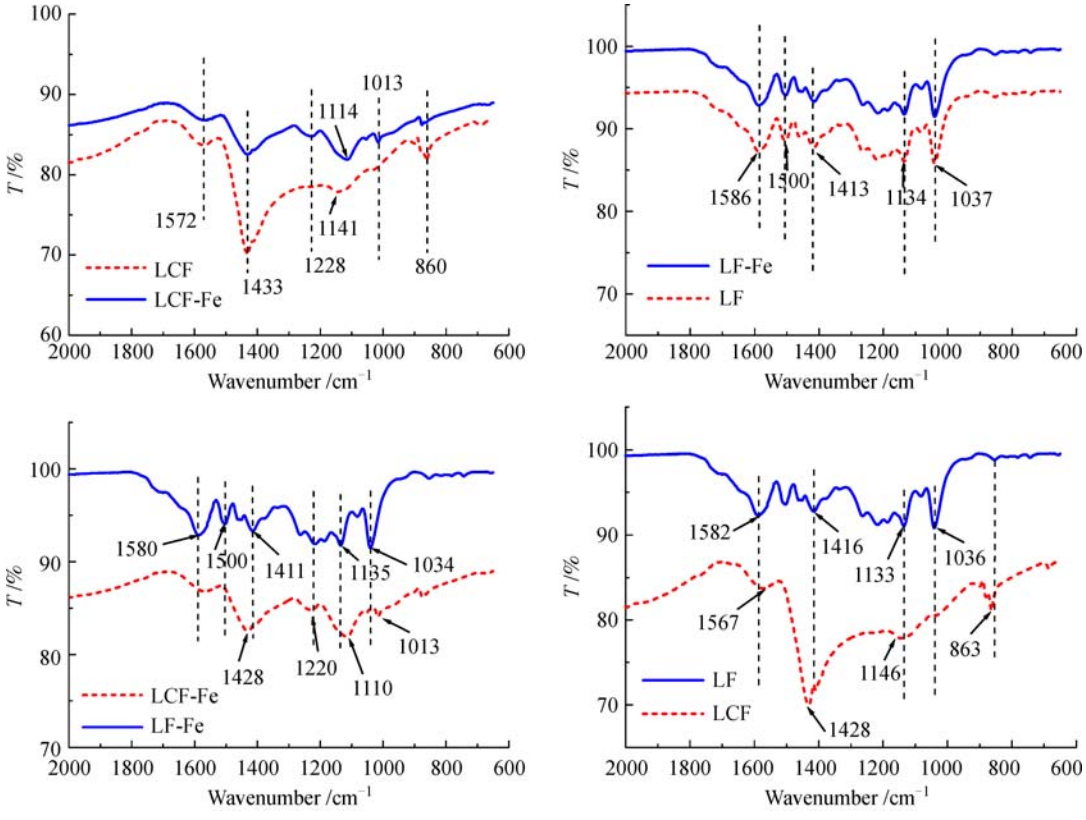

Fig. 2 The FTIR spectrum curves of LF, LF-Fe, LCF, and LCF-Fe

is assigned to C–O structures. After activation, the band at 1065 cm^{-1} mostly disappears. The increase of peaks intensities at 1470 cm^{-1} represents the vibration of C–H in CH_3 and CH_2, respectively. Characteristic bands observed at 1500 and 1600 cm^{-1} represented the C = C aromatic skeletal vibrations of lignin. The two typical adsorption peaks located at 1260 and 876 cm^{-1} are contributed by the guaiacyl groups of lignin. Therefore, the prepared carbon fibers are mainly composed of different oxygen-containing groups, such as hydroxyl, carboxyl, guaiacyl functionalities, etc. These functional groups could exhibit effect on the surface properties of carbon fibers, thus, influence their adsorption characteristics. In general, much more oxygen containing function groups will decrease VOC adsorption for nonpolar compounds and increase water vapor adsorption. Both are detrimental to the performance of activated carbon.

Activation of the carbonized fibers produces the pores, an increase of the carbon content and lower oxygen content. The pore size distribution of the lignin-based carbon fiber adsorbents were determined using nitrogen adsorption isotherms data at 77 K. Table 2 summarizes the

Table 2 Physicochemical characteristics of LCF and LCF-Fe

Characteristics		Adsorbents	
		LCF	LCF-Fe
Pore structure	S_{BET} /($m^2 \cdot g^{-1}$)	117	1466
	Average pore diameter /nm	6.99	2.43
	Total volume /($cm^3 \cdot g^{-1}$)	0.20	0.89
	Micropore volume /($cm^3 \cdot g^{-1}$)	0.02	0.52
Surface chemistry	Elementary analysis C/H/N/O (wt-%)	62.31/4.14/0.56/6.87	67.08/1.54/3.65/2.48
	pH_{PZC}	6.87	6.03

properties of BET surface areas and micropore volumes of the prepared adsorbents. BET analysis was also used to measure the micropore surface area. The results illustrate that the BET surface areas and total pore volume of the carbon fibers increased dramatically after activation using Fe_3O_4. Accordingly, increases in BET surface area were primarily attributable to increases in micropore volume. The surface area of the carbon adsorbent was increased from 117 to 1466 m^2/g by using Fe_3O_4 as an activation catalyst. The micropore volume increased from 10% to 58% after activation using Fe_3O_4. The N_2 adsorption isotherms of LCF and LCF-Fe presented in Fig. S1 show that an obvious increase in the nitrogen uptake and porosity of adsorbents was presented after activating with Fe_3O_4.

The nitrogen sorption isotherm of LCF-Fe and LCF are shown in Fig. S1. The nitrogen sorption isotherms for LCF-Fe are Type I according to the IUPAC classification. A large amount of nitrogen adsorption occurs in a relative low pressure range, and the adsorption capacity increases with increasing pressure. However, our LCF sample had some hysteresis and could be classified as an IUPAC Type IV isotherm. N_2 adsorption in the low-relative-pressure range ($< 0.2\ P/P_0$) is associated with micropores, whereas adsorption at the high relative pressure range ($> 0.8\ P/P_0$) originates from mesopores. A pore volume-pore surface area distribution curve is shown in Fig. 3.

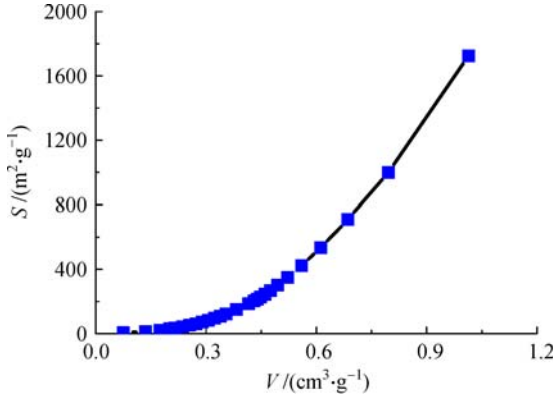

Fig. 3 The surface area versus pore volume computed from the N_2 isotherm of LCF-Fe

Figure 4 depicts micropore and mesopore size distribution for LCF-Fe and LCF. LCF-Fe micropores are concentrated in an area ranging approximately from 0.5–0.6 nm; concentrated LCF micropores are span a range of 1–2 nm with a lower pore volume. Concentrated LCF-Fe mesopores span an approximated range of 2–5 nm; concentrated LCF mesopores coffer different areas ranging from 12–16 nm and 2–5 nm. The pore size distribution results illustrate that for LCF, mesoporous characteristics are dominant. The average pore diameters of LCF-Fe are 6.99 nm. However, a lot of micropores were formed when Fe_3O_4 was added, and the average pore diameters decreased from 6.99 to 2.43 nm.

Elemental analysis and pH_{PZC} for the LCF and LCF-Fe are also summarized in Table 2. The surface hydrophobicity of an adsorbent is related to the amount of surface oxygen-containing functional groups. The amount of surface oxygen containing functional groups exhibits the effect of hydrophobicity of the adsorbents. The much lower oxygen content exhibits the much higher hydrophobicity. LCF-Fe has much lower oxygen content than LCF, suggesting more hydrophobic surface. Table 2 clearly shows that LCF-Fe has a more hydrophobic surface than that of LCF. The variations of pH_{PZC} reflect changes in the ratio between the acidic and basic surface groups. The use of Fe_3O_4 as an activation catalyst lowered the pH_{PZC} slightly; however, the lowered pH_{PZC} was also due to a decrease in the oxygen-containing functional groups, which is consistent with element analysis results.

3.2 Single solute adsorption

The adsorption capacities of toluene on LCF-Fe under room temperature (ca. 20 °C) were measured. Figure 5(a) shows the adsorption isotherm of toluene on LCF-Fe under room temperature (ca. 20 °C). The experimental adsorption isotherm data for toluene on LCF-Fe are represented as symbols and fitted with the D-R equation in Fig. 5(b). The experimental data fit the D-R equation well with a correlation coefficient of $R^2 = 0.975$. The constants were obtained by plotting the ln(W) *versus* $[\ln(P_0/P)]^2$ in the D-R equation. The maximum adsorption space, W_0 and microporosity constant, B are estimated 0.51 $cm^3/g \cdot m$

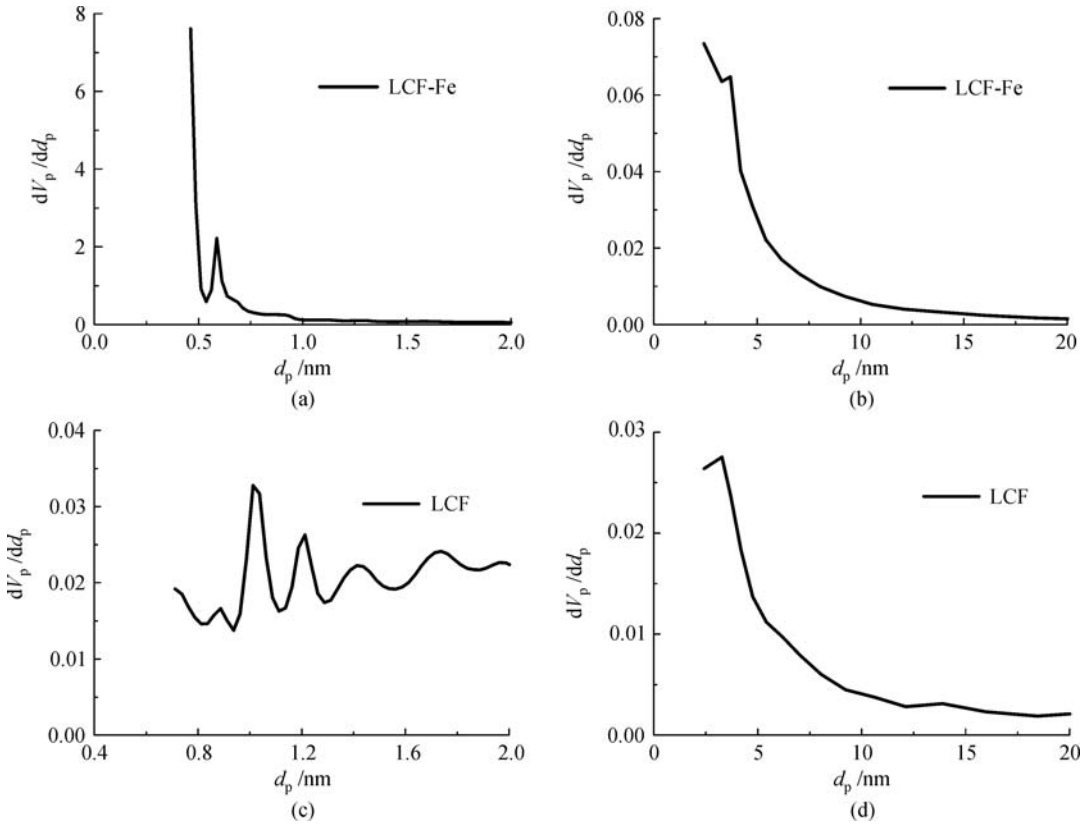

Fig. 4 Pore size distributions of LCF-Fe and LCF. Micropores and mesopores were obtained from Barrett-Joyner-Halenda and HK analysis of the nitrogen desorption branch, respectively

(which is close to the micropore volume that was estimated using the nitrogen isotherm, 0.52 cm^3/g) and 3.79×10^{-7} mol^2/cal^2, respectively. For the similar surface area and initial concentration, the adsorption capacity of 439 mg/g for LCF-Fe is close to the commercial activated carbon fiber, which has been determined to be 500 mg/g [25].

3.3 The competitive interaction between water vapor and toluene vapor

3.3.1 The impact of humidity on adsorption capacity

Water vapor reduces the amount of VOCs that can be

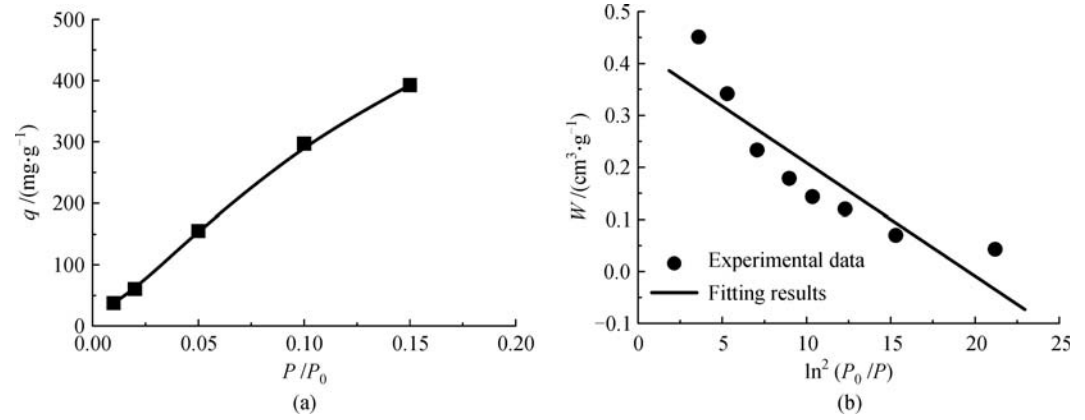

Fig. 5 (a) Adsorption isotherm for single toluene on LCF-Fe at 298 K and (b) experimental data for the adsorption of toluene on LCF-Fe

adsorbed on carbon fibers by filling the micropores with water. The water-filled micropores do not adsorb VOC (or adsorb very little VOC). In order to determine the amount that can be adsorbed, it is necessary to determine the amount of surface area that is covered by water, and water vapor isotherms are conducted to determine this. Previous studies [26] have found that adsorption of water vapor increases with increasing oxygen content of the carbon surface [27]. Water vapor adsorption isotherms for relative humidities between 0% and 90% were tested and are shown in Fig. S2. Significant water vapor adsorption did not occur until 70% RH for LCF and LCF-Fe. LCF-Fe exhibited a sharper increase in adsorption capacity in comparison to LCF for RH between 70% and 90%. This increase suggests that LCF-Fe exhibits much higher adsorption capacity for water vapor than LCF at the 70% to 90% RH range, which may be attributed to hydrophilic surface functional groups and the presence of more micropore volume. These results indicate that water vapor adsorption will have a significant impact on VOC adsorption at RH values greater than 70%.

3.3.2 Impact of RH on the adsorption of VOCs

The adsorption of VOCs in the presence of water vapor is quite different from that under dry conditions [28]. Adsorption isotherms of toluene on LCF-Fe were measured at an RH of 20%, 50%, and 80%. Figure 6 shows the experiment isotherms data (data points) for the LCF-Fe at different RHs along with the corresponding Okazaki model predictions (solid lines) for 20%, 50%, 60%, 70% and 80%. Based on these results, high RH reduces the adsorption capacity of toluene, and it follows the trend of increasing adsorption capacity of water vapor (which covers more adsorption surface area. A slight slope change of the isotherm curves was found when the RH increased from 0% to 50%, suggesting less inhibition effect and a lower water capacity on the LCF-Fe. However, when the RH is higher than 50%, RH exhibited a sharper increase in adsorption capacity, indicating that water vapor can have a significant impact on toluene adsorption. When the RH gets to 80%, water vapor adsorption is close to saturated values, which can have a serious effect on the adsorption equilibrium.

3.3.3 The model for predicting the adsorption of toluene and water vapor

Okazaki proposed that organic vapors are adsorbed onto the carbon adsorbents by these three mechanisms: (1) adsorption on dry surface, (2) adsorption on wet surface, and (3) dissolution in condensed water [29]. The total capacity of the carbon adsorbents for the toluene is the sum of the three components. Detailed descriptions about the model are shown in the supporting information.

3.4 The comparison of experimental results and prediction values

To predict the adsorption equilibria, the adsorption isotherm of solvent (Fig. 5), the adsorption and desorption isotherm of water (Fig. S2) and the aqueous phase isotherm (Fig. S3) are used. The results presented by the Okazaki model are listed in Table S2. The toluene dissolved in condensed water (q_{o2}) was small, which is negligible. The contribution for aqueous phase adsorption (q_{o3}) is less if the RH values are lower than 50%, but when RH values exceed 50%, the contribution for aqueous phase adsorption will take a higher proportion for the total adsorption capacity. The water vapor initiates the competitive interaction with single organic vapor; however, the adsorption kinetics will not allow much to be adsorbed in the water filled pores in a gas phase application.

The comparisons of the predicted and experimental results are shown in Fig. 6 and Table S2. Table S2 gives the average relative deviation (ARD) between predicted and observed data. As for the RH of 20% and RH of 50%, the ARD are 5.04% and 7.41%, respectively. However, the ARD value approaches 12.99% when the RH value approaches 80%. In conclusion, the results demonstrate that the model exhibits the satisfactory predictions of the data.

3.5 CPHSDM prediction

The rate of adsorption is usually limited by mass transfer and influenced by the adsorbate and adsorbent. The developments of mathematical models, which describe adsorption kinetics, are derived from mass transfer rate expressions. The constant pattern homogeneous surface diffusion model (CPHSDM) provide mechanistic insight and predict breakthrough curves instead of using long duration pilot tests.

LCF-Fe is fiber and its external mass transfer is limited. Intraparticle diffusion is very fast. It would be good to run the model for external mass transfer control. It is necessary to calculate gas phase diffusivity (D_g) to get the S_t and k_f. The Wilke-Lee modification of Hirschfelder, Bird-Spotz correlation can be used to calculate the diffusivity of an organic compound in the gas-phase. The detailed calculation procedures are listed in the supporting information.

The breakthrough curves for toluene in the air of LCL-Fe and Calgon BPL was calculated using the pore surface diffusion model with AdDesignSTM Version 1.0.45 (Michigan Technological University). The toluene prediction breakthrough curves were conducted with a series of parameters, which are shown in Table S3. The diameter of Calgon BPL and LCF-Fe used in this study was 3.7 and 5.0 cm, respectively. The adsorber properties are as follows: Bed length: 1.2 m; bed diameter: 3 m; activated carbon mass: 3800 kg; EBCT: 6.52 s; $C_0 = 0.45$ mg/L; Flow rate: 1.3 m^3/s; $\mu_{air} = 1.8 \times 10^{-5}$ (Ns)/m^2; $D_{air} = 8.4 \times$

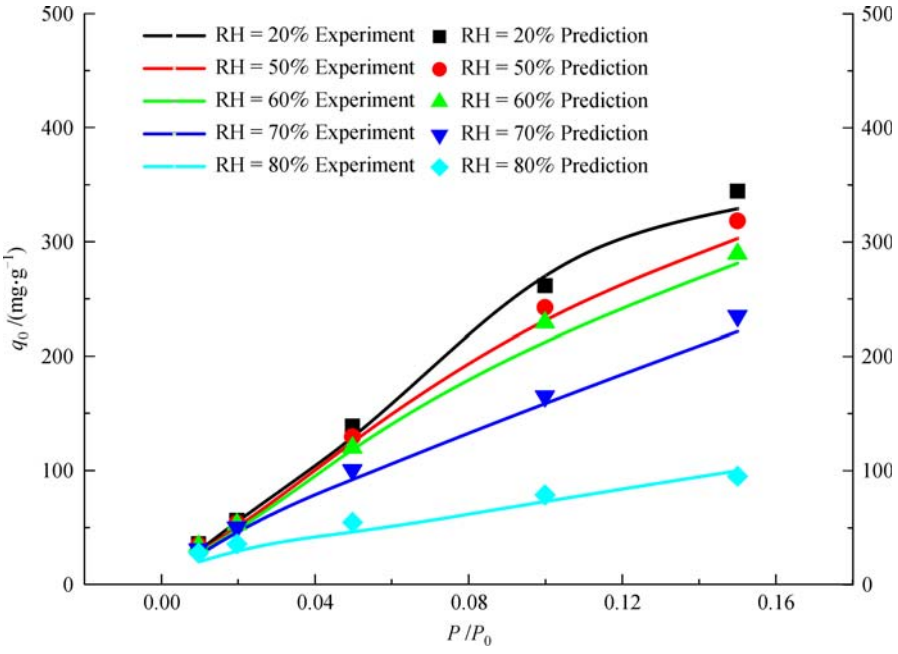

Fig. 6 Experimental data for adsorption of toluene in the presence of water vapor compared to thermodynamic model predictions

10^{-6} m^2/s; ρ_{air} = 1.17 kg/m^3. Gnielinski correlation was used for the estimates of the external mass transport coefficient, which are shown in the supporting formation.

Figure 7 presents the toluene breakthrough curves of LCF-Fe and Calgon BPL that were predicted by CPHSDM. In LCL-Fe group, the outlet toluene concentration began to rise after 28 d, while the breakthrough was completed within 18 d in the Calgon BPL group. Therefore, the LCL-Fe exhibited the better performance for removing toluene from air than Calgon BPL in the breakthrough prediction. As shown in Table 3, the adsorption capacity of LCL-Fe for toluene was 412 mg/g, which is twice that of Calgon BPL. Therefore, the lignin based carbon fiber is projected as an alternative procedure that can be used to remove VOCs, which is cheaper when using renewable biomass.

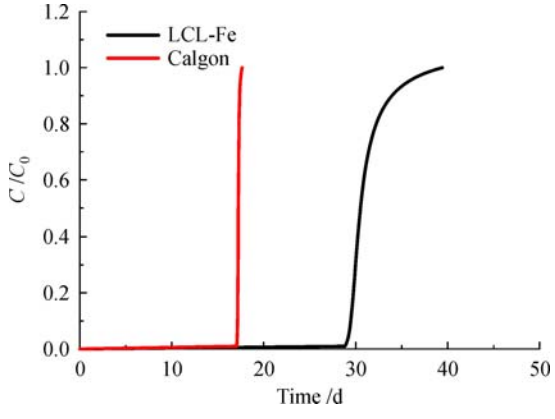

Fig. 7 CPHSDM predictions for toluene breakthrough curves of LCF-Fe and Calgon BPL

Table 3 The adsorptive capacities of LCF-Fe and commercial GACs during the column tests

Adsorbents	Time[a)] /h	Bed volume[a)]	Toluene removed /kg	Adsorption capacity /(mg·g^{-1})
LCL-Fe	946	522023	1566	412
Calgon BPL	74.6	41147	867	228

a) The exhaustion point of C/C_0 = 1

4 Conclusions

Two types of lignin based carbon fibers (LCF-Fe and LCF) were prepared using electrospinning. The surface area of the LCF increased from 117 to 1466 m^2/g when Fe_3O_4 was added. Adsorption isotherms were measured for toluene under dry and humid conditions on LCF-Fe adsorbents. For a similar surface area, the adsorption capacity of 439 mg/g for LCF-Fe is close to the commercial activated carbon fiber of 500 mg/g under dry conditions. The D-R equation fits of toluene adsorption isotherm data reasonably well. Water vapor adsorption was not significant for the LCF and LCF-Fe activated carbons until relative humidities rose above 70%. Based on the adsorption isotherm of toluene-water vapor under different humidities, if the humidity was lower than 50%, RH exhibited little effect on adsorption capacity. When the RH was 80%, water nearly filled all the pores and significantly reduced

the adsorption capacity. The Okazaki model exhibits satisfactory predictions of the toluene adsorption capacity at different humidities. The CPHSDM was further used to predict breakthrough profiles.

Nomenclature

$1/n$	Freundlich constant, −
β	affinity coefficient of the adsorbate, −
p	pressure, kPa
p_o	saturated vapor pressure, kPa
q	amount adsorbed, mg/g-carbon
R	gas constant, cc·mmHg/mol·K
r	pore radius, cm, Å
S	surface area, m^2/g-carbon
S_C	surface area of wet surface, m^2/g-carbon
S_D	surface area of dry surface, m^2/g-carbon
S_T	total surface area, m^2/g-carbon
T	temperature, K
V	volume, mL
V_C	volume of condensed phase, mL/g-carbon
ρ	density, g/mL
Subscripts	
o	solvent
w	water
1	adsorption on dry surface
2	dissolution into condensed phase
3	liquid-phase adsorption onto wet suface
ε_p	particle porosity
ε	bed porosity

Acknowledgements The authors are grateful for the National Natural Science Foundation of China (Grant No. 51576048). Thanks to the financial support of Jiangsu Province Environmental Protection Foundation (2015013), the Industry, Education, and Research Prospective Project of Jiangsu Province (BY2015060-04) and Fok Ying Tong Education Foundation (142026). This research was also supported by the Brook Byers Institute for Sustainable Systems, Hightower Chair, and the Georgia Research Alliance at the Georgia Institute of Technology.

Electronic Supplementary Material Supplementary material is available in the online version of this article at http://dx.doi.org/10.1007/s11705-017-1646-y and is accessible for authorized users.

References

1. Lillo-Ródenas M A, Cazorla-Amorós D, Linares-Solano A. Behaviour of activated carbons with different pore size distributions and surface oxygen groups for benzene and toluene adsorption at low concentrations. Carbon, 2005, 43(8): 1758–1767
2. Gupta V K, Verma N. Removal of volatile organic compounds by cryogenic condensation followed by adsorption. Chemical Engineering Science, 2002, 57(14): 2679–2696
3. Das D, Gaur V, Verma N. Removal of volatile organic compound by activated carbon fiber. Carbon, 2004, 42(14): 2949–2962
4. Long C, Liu P, Li Y, Li A, Zhang Q. Characterization of hydrophobic hypercrosslinked polymer as an adsorbent for removal of chlorinated volatile organic compounds. Environmental Science & Technology, 2011, 45(10): 4506–4512
5. Sullivan P, Moate J, Stone B, Atkinson J D, Hashisho Z, Rood M J. Physical and chemical properties of PAN-derived electrospun activated carbon nanofibers and their potential for use as an adsorbent for toxic industrial chemicals. Adsorption, 2012, 18(3-4): 265–274
6. Hashisho Z, Emamipour H, Rood M J, James Hay K, Kim B J, Thurston D. Concomitant adsorption and desorption of organic vapor in dry and humid air streams using microwave and direct electrothermal swing adsorption. Environmental Science & Technology, 2008, 42(24): 9317–9322
7. Foster K L, Fuerman R G, Economy J, Larson S M, Rood M J. Adsorption characteristics of trace volatile organic compounds in gas streams onto activated carbon fibers. Chemistry of Materials, 1992, 4(5): 1068–1073
8. Qiao W M, Huda M, Song Y, Yoon S H, Korai Y, Mochida I, Katou O, Hayashi H, Kawamoto K. Carbon fibers and films based on biomass resins. Energy & Fuels, 2005, 19(6): 2576–2582
9. Carrott P J M, Carrott M M L R. Lignin-from natural adsorbent to activated carbon: A review. Bioresource Technology, 2007, 98(12): 2301–2312
10. Hayashi J, Kazehaya A, Muroyama K, Watkinson A P. Preparation of activated carbon from lignin by chemical activation. Carbon, 2000, 38(13): 1873–1878
11. Ruiz-Rosas R, Bedia J, Lallave M, Loscertales I G, Barrero A, Rodríguez-Mirasol J, Cordero T. The production of submicron diameter carbon fibers by the electrospinning of lignin. Carbon, 2010, 48(3): 696–705
12. Ahmad J J, Babak K, Nemat J, Roshanak R K, Mehdi A, Ali A B. Fenton-like catalytic oxidation of tetracycline by AC@Fe_3O_4 as a heterogeneous persulfate activator: Adsorption and degradation studies. Journal of Industrial and Engineering Chemistry, 2017, 45: 323–333
13. Chiang Y C, Chiang P C, Huang C P. Effects of pore structure and temperature on VOC adsorption on activated carbon. Carbon, 2001, 39(4): 523–534
14. Lordgooei M, Kim M S. Modeling volatile organic compound sorption in activated carbon. I: Dynamics and single-component equilibrium. Journal of Environmental Engineering, 2004, 130(3): 212–222
15. Cosnier F, Celzard A, Furdin G, Bégin D, Marêché J F. Influence of water on the dynamic adsorption of chlorinated VOCs on active carbon: Relative humidity of the gas phase versus pre-adsorbed water. Adsorption Science and Technology, 2006, 24(3): 215–228
16. Kim T Y, Kim S J, Cho S Y. Effect of relative humidity on the adsorption characteristics of carbon tetrachloride in a fixed bed. Journal of Industrial and Engineering Chemistry, 2004, 10(2): 188–195
17. Russell B P, LeVan M D. Coadsorption of organic compounds and

water vapor on BPL activated carbon. 3. Ethane, propane, and mixing rules. Industrial & Engineering Chemistry Research, 1997, 36(6): 2380–2389

18. Marban G, Fuertes A B. Co-adsorption of *n*-butane/water vapour mixtures on activated carbon fibre-based monoliths. Carbon, 2004, 42(1): 71–81
19. Kaplan D, Nir I, Shmueli L. Effects of high relative humidity on the dynamic adsorption of dimethyl methylphosphonate (DMMP) on activated carbon. Carbon, 2006, 44(15): 3247–3254
20. Ryu Y K, Lee H J, Yoo H K, Lee H C. Adsorption equilibria of toluene and gasoline vapors on activated carbon. Journal of Chemical & Engineering Data, 2002, 47(5): 1222–1225
21. El-Sharkawy I I, He J M, Ng K C, Yap C, Saha B B. Adsorption equilibrium and kinetics of gasoline vapors onto carbon-based adsorbents. Journal of Chemical & Engineering Data, 2007, 53(1): 41–47
22. Brosillon S, Manero M H, Foussard J N. Mass transfer in VOC adsorption on zeolite: Experimental and Theoretical Breakthrough Curves. Environmental Science & Technology, 2001, 35(17): 3571–3575
23. Díez N, Álvarez P, Granda M, Blanco C, Santamaría R, Menéndez R. A novel approach for the production of chemically activated carbon fibers. Chemical Engineering Journal, 2015, 260: 463–468
24. Song M, Jin B, Xiao R, Yang L, Wu Y M, Zhong Z P, Huang Y J. The comparison of two activation techniques to prepare activated carbon from corn cob. Biomass and Bioenergy, 2013, 48: 250–256
25. Yun J H, Hwang K Y, Choi D K. Adsorption of benzene and toluene vapors on activated carbon fiber at 298, 323, and 348 K. Journal of Chemical & Engineering Data, 1998, 43(5): 843–845
26. Wood G O. Affinity coefficients of the Polanyi/Dubinin adsorption isotherm equations: A review with compilations and correlations. Carbon, 2001, 39(3): 343–356
27. Stoeckli F, Lavanchy A. The adsorption of water by active carbons, in relation to their chemical and structural properties. Carbon, 2000, 38(3): 475–477
28. Crittenden J C, Rigg T J, Perram D L, Tang S R, Hand D W. Predicting gas-phase adsorption equilibria of volatile organics and humidity. Journal of Environmental Engineering, 1989, 115(3): 560–573
29. Okazaki M, Tamon H, Toei R. Prediction of binary adsorption equilibria of solvent and water vapor on activated carbon. Journal of Chemical Engineering of Japan, 1978, 11(3): 209–215
30. Defay R, Prigogine I, Bellemans A. Surface Tension and Adsorption. New York: Longman, 1966
31. Crittenden J C, Cartright P D, Rick B, Tang S R, Perram D L. An Evaluation of the Technical Feasibility of the Air-Stripping Solvent Recovery Process. Denver: American Water Works Association Research Foundation, 1987